Optics and Lasers in Engineering 129 (2020) 106050

Contents lists available at ScienceDirect

Optics and Lasers in Engineering

journal homepage: www.elsevier.com/locate/optlaseng

SPGD and Newton iteration mixed algorithm used in freeform surface metrology

Yu Zhang [a,b,*], Xiaobo Tian [c], Rongguang Liang [c,*]

[a] Institute of Materials Physics, College of Science, Northeast Electric Power University, Jilin, Jilin 132012, China
[b] State Key Laboratory of Applied Optics, Changchun Institute of Optics, Fine Mechanics and Physics, Chinese Academy of Sciences, Changchun, Jilin 130022, China
[c] College of Optical Sciences, University of Arizona, Tucson, AZ 85721, USA

ARTICLE INFO

Keywords:
Stochastic parallel gradient descent algorithm
Newton iteration algorithm
Deformable mirror
Freeform surface
Optimization

ABSTRACT

Freeform surfaces are widely used in advanced optical systems. In order to accurately measure freeform surfaces, an adaptive interferometer with deformable mirror (DM) has been developed for the freeform surface metrology. To ensure the efficiency, a stochastic parallel gradient descent (SPGD) and Newton iteration mixed algorithm to drive the DM has been proposed, it can achieve the minimum value of the optimization and is suitable for the different interferograms. The simulation and experimental results verify the correctness and feasibility of the proposed DM driving algorithm.

1. Introduction

Compared with traditional spherical and aspherical elements, freeform surface has more degrees of freeform for correcting optical aberrations and controlling ray directions [1], enabling simple and compact optical systems with high performance. In recent years, a number of advanced manufacturing technologies have been developed to manufacture the highly accurate optical freeform surface [2].

During the manufacturing process, the freeform surface needs to be tested to ensure the manufacturing accuracy. Although the interferometry is the industry standard and has been used for freeform surface metrology [3–5], for freeform surfaces with large departure from the spherical surface, the special computer generated hologram (CGH) [6] or null lens is needed for each surface under test, it is time-consuming and expensive, hence, it is not suitable for the freeform surface in-situ metrology. At present, the scanning technologies, including coordinate measuring machines (CMMs) [7], profilometers [8] and confocal microscopy [9] have been widely used in in-situ metrology. While these methods can test various types of surfaces, there are some limitations. For contact metrology such as CMMs and profilometers, the measurement process is relatively long and the measurement accuracy is easy to be affected by the environmental factors, such as vibration, in addition, the contact probe may damage the optical surface. For the confocal microscopy, the measuring range and vertical resolution are limited by the numerical aperture of the objective, laser wavelength, and the sensitivity of the piezo-transducer (PZT) used.

To improve the performance of the interferometer and scanning technology, the adaptive interferometer [10–12] with deformable mirror (DM) has been developed, it can quickly and accurately test the optical freeform surface without using CGH and null lens.

For the adaptive interferometer, the control algorithm of DM is essential. In 1998, the stochastic parallel gradient descent (SPGD) algorithm was first designed [13], and widely used in the adaptive optics [14–17]. In 2016, [11] researched the SPGD algorithm used in the adaptive interferometer, the SPGD algorithm is effective even if the phase can't be calculated by the interferogram, there are three steps of optimaztions in all, the first step used the sum-of-squares of the difference of grayscale values between two adjacent pixels in the dark region without fringe as the system performance metric, the second and third steps used the RMS value of phase as the system performance metric, the simulated and experimental results were well evaluated, but if the fringe density of the interferogram is too large after the first optimazation, the phase also can't be calculated, hence the RMS value of phase can't be set as the system performance metric in the second step, especially for the complex freeform surface, moreover, in the final step, the optimized result of SPGD algorithm can't be achieved to a minimum value. Newton iteration algorithm can achieve the minimum value of the optimization, and it can converge after only two or three iterations, however, the optimization speed will be affected since the variables of the DM is large. Hence, in the adaptive freeform surface metrology, single control algorithm is difficult to control the DM effectively, the integrated algorithm is essential to drive the DM.

In this paper, we will discuss the SPGD and Newton iteration mixed algorithm used for the DM control in the adaptive freeform

* Corresponding authors.
E-mail addresses: 521zhangyu2008@163.com (Y. Zhang), rliang@optics.arizona.edu (R. Liang).

https://doi.org/10.1016/j.optlaseng.2020.106050
Received 2 November 2019; Received in revised form 19 December 2019; Accepted 30 January 2020

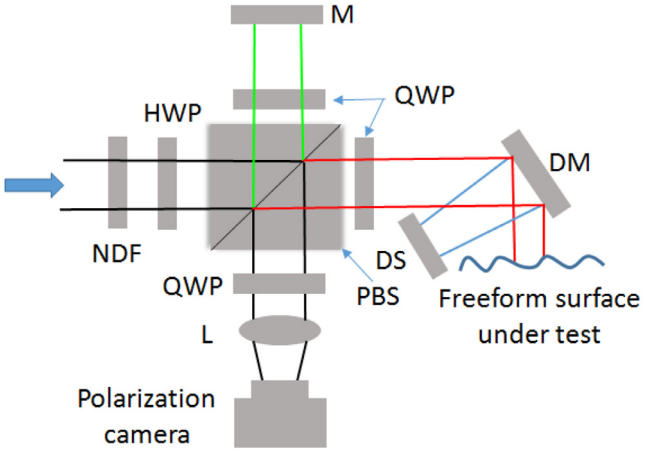

Fig. 1. Schematic layout of the adaptive interferometer: NDF, neutral density filter; HWP, half-wave plate; PBS, polarization beam splitter; QWP, quarter-wave plate; L, lens; M, mirror; DM, deformable mirror; DS, deflectometry system.

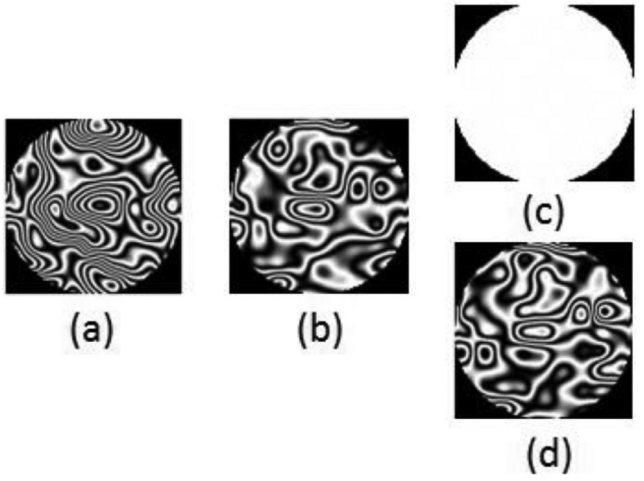

Fig. 2. Simulated interferograms between the second and final steps when the tested phase distribution is generated by the response matrix of DM. (a) The original interferogram, (b) the interferogram after using SPGD algorithm (second step), (c) and (d) the final interferogram after further using Newton iteration and SPGD algorithms (final step).

surface metrology. Section 2 presents the principle of the adaptive interferometer, then, the driving algorithm of DM is introduced in Section 3. In Section 4, the simulation of driving algorithm is discussed, Section 5 evaluates the driving algorithm with the experimental data. Finally, the conclusion is drawn in Section 6.

2. Principle of adaptive interferometer

The schematic layout of the adaptive interferometer is shown in Fig. 1. The light is attenuated by the neutral density filter (NDF) and its polarization direction is tuned by a half-wave plate (HWP) to adjust the fringe contrast of the interferogram, then p polarization and s polarization beams are transmitted and reflected from the polarization beam splitter (PBS) respectively, serving as the test wave (red line) and the reference wave (green line), the reference arm includes a quarter-wave plate (QWP) and a reference mirror, and the test arm includes a QWP, a deformable mirror (DM) which can change the test wavefront. The reflected test beam and reference beam are transformed to oppositely circularly polarized after passing through the QWP and interfere at the focal plane of the polarization camera. 4-frame phase shifted interferograms can be obtained simultaneously without the physical phase shift [18]. The adaptive interferometer also can test the aspherical surface, the reference wavefront can be adjusted to the spherical wavefront using the objective.

When the tested optics is a freeform surface, we may obtain the initial interferogram with dark region without fringe or dense fringe area since the surface departure from spherical surface could exceed the measuring range of the interferometer when the DM is flat. Therefore we need to drive the DM to generate approximate no-fringe interferogram to get the accurate phase without large retrace errors in the interferometer data. With the surface shape of the DM measured by the deflectometry system (DS) [19,20], we can obtain the phase distribution of the freeform surface W_F using the tested phase distribution W_T obtained by the adaptive interferometry and phase distribution of the DM W_{DM}.

3. Driving algorithm of DM

SPGD algorithm is a very mature algorithm and usually used to drive the DM in adaptive optics. However, single control algorithm is difficult to effectively control the DM in the adaptive interferometer, hence, the integrated algorithm which mixes the SPGD and Newton iteration algorithms is introduced to address the limitations of single SPGD algorithm, such as the number of iterations is relatively large and the result can't be optimized to a minimum value.

SPGD algorithm evaluates the control voltage gradient by the small random perturbations of control voltages and the variation of system performance metric, searches and iterates in the gradient direction to optimize system performance metric. The optimization process is in the following:

1) Initialize the voltage $U = U_0$, $U_0 = (0, 0, \cdots, 0)$;
2) generate random turbulence voltage δU with the mean as zero, and δU needs to satisfy Bernoulli distribution;
3) establish the system performance metric J;
4) add random turbulence voltage to the control voltage to obtain $U + \delta U$ and drive the DM;
5) obtain the value of the system performance metric

$$J_+ = J(U + \delta U). \tag{1}$$

6) add random turbulence voltage to the control voltage to obtain $U - \delta U$ and drive the DM;
7) obtain the value of the system performance metric

$$J_- = J(U - \delta U). \tag{2}$$

8) calculate the control voltage for next iteration, and drive the DM

$$U' = U - \gamma(J_+ - J_-)\delta U. \tag{3}$$

where γ is the gain coefficient. When the system performance metric is optimized to the minimum value, the gain coefficient γ is positive, otherwise it is negative.

1) repeat 4) to 8) until the result meets the convergence condition.

At the beginning, there may exist relatively dark region with only background intensity and no fringe in the interferogram, so before we apply SPGD algorithm, we need to establish the system performance metric J as

$$J = \sum_{all(i,j)} I(i, j). \tag{4}$$

where $I(i, j)$ is the grayscale value of one pixel in the relatively dark region without fringe, J represents the sum of the grayscale values in this region.

For the regions without fringe due to the large surface departure from spherical surface, the value of J will be very small because those regions with only background intensity are relatively dark. The value of J will increase when fringes appear and become more dense. During the

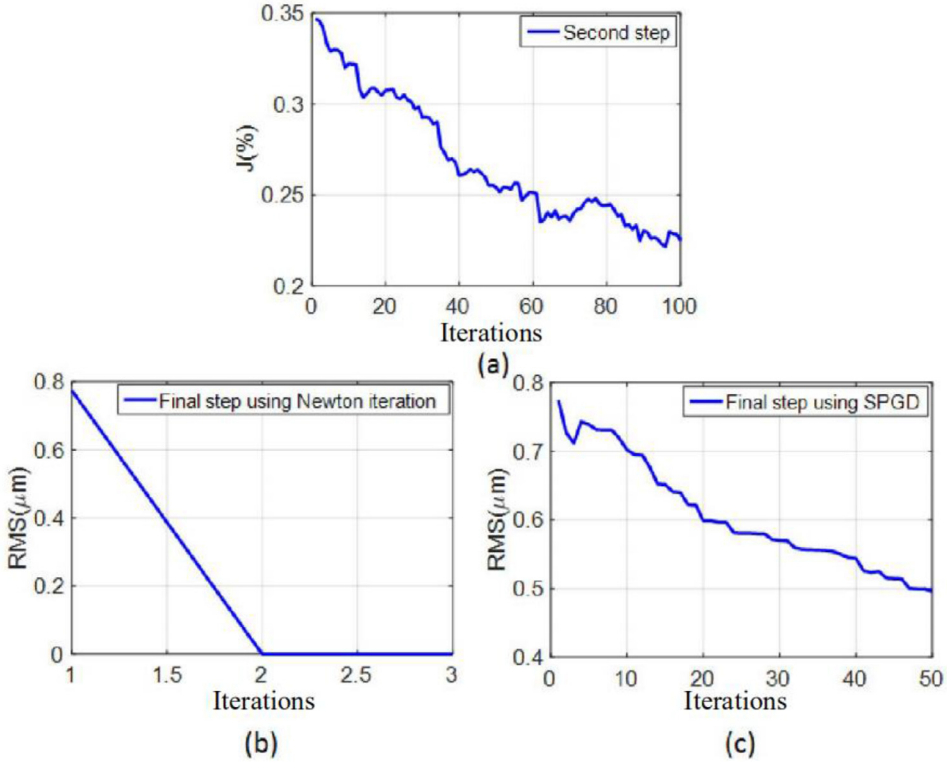

Fig. 3. Simulated convergence curves between the second and final steps when the tested phase distribution is generated by the response matrix of DM. (a) The convergence curve using SPGD algorithm (second step), (b) and (c) the convergence curves using Newton iteration and SPGD algorithms (final step).

fringe search, the voltage of the actuators will be updated until J meets the convergence condition which depends on the practical situation.

The fringes are typically very dense when they are recovered in the previously dark regions since the entire metrology system is largely deviated from the null condition. The second step is needed to relax the whole fringe density. In this step, SPGD algorithm will be used in the whole interferogram, and the system performance metric J needs to be reset as Eqs. (5)–(8).

$$I'(i,j) = I(i,j) - I_{mean}. \tag{5}$$

$$Num1 = Count\begin{pmatrix} \left(\left(I'(i,j)>0\right)\&\&\left(I'(i,j+1)<0\right)\right) \\ \| \left(I'(i,j)<0\right)\&\&\left(I'(i,j+1)>0\right) \end{pmatrix}. \tag{6}$$

$$Num2 = Count\begin{pmatrix} \left(\left(I'(i,j)>0\right)\&\&\left(I'(i+1,j)<0\right)\right) \\ \| \left(I'(i,j)<0\right)\&\&\left(I'(i+1,j)>0\right) \end{pmatrix}. \tag{7}$$

$$J = \left(\frac{Num1}{2} + \frac{Num2}{2}\right)/Num. \tag{8}$$

where *Num* is the number of the effective points, before the interferogram optimization, the effective domain of the interferogram needs to be identified, or a mask needs to be made to obtain the effective domain, the points in the effective domain are the effective points, $I(i, j)$ is the grayscale value of one pixel, I_{mean} is the mean of all $I(i, j)$, $I'(i, j)$ is the grayscale value after subtracting I_{mean}, *Num* 1 is the number that negative or positive symbols of $I'(i, j)$ and $I'(i, j+1)$ are different, *Num* 2 is the number that negative or positive symbols of $I'(i, j)$ and $I'(i+1, j)$ are different, and J represents the proportion of the number of the different symbols to the number of the effective points in the interferogram.

In the second step, the driving voltage of the DM actuators are tuned to reduce the fringe density. The proportion which represents the fringe density is used as the system performance metric J, and the gain coefficient γ in Eq. (3) can be set as a constant for the different fringe density. If the number of the different symbols is set as the system performance metric, γ may need to be set as a variable due to the different situations, hence, the proportion is more suitable than the number of the different symbols to be the system performance metric.

After the second step, the RMS value of the tested phase distribution can be used as the system performance metric since it can be calculated from the phase shifted interferograms with relatively sparse fringes. If SPGD algorithm is still used, it is difficult to reduce the RMS value to a minimum value because the interferogram can't be optimized to approximate no-fringe after the iteration converges, when the fringe density is relatively large and there is large noise in the interferogram, the accurate result couldn't be obtained finally. To address this limitation, the Newton iteration algorithm [21] is used to further fine tune the voltage of the actuators to obtain approximate no-fringe interferogram.

The Newton iteration algorithm is

$$Z_{n+1} = Z_n - \frac{f(Z_n)}{f'(Z_n)} = Z_n + \Delta Z_n. \tag{9}$$

where Z_n is the voltage of the actuators in every iteration, Z_{n+1} is the new voltage of the actuators after every iteration, $f(Z_n)$ is the tested phase distribution in every iteration, and $f'(Z_n)$ is the partial derivative of $f(Z_n)$, ΔZ_n is the variation of the voltage.

$$J = f'(Z_n) = \frac{\partial(f_1, f_2, \cdots, f_l)}{\partial(z_1, z_2, \cdots, z_k)} = \begin{bmatrix} \frac{\partial f_1}{\partial z_1} & \frac{\partial f_1}{\partial z_2} & \cdots & \frac{\partial f_1}{\partial z_k} \\ \frac{\partial f_2}{\partial z_1} & \frac{\partial f_2}{\partial z_2} & \cdots & \frac{\partial f_2}{\partial z_k} \\ \vdots & \vdots & \ddots & \vdots \\ \frac{\partial f_l}{\partial z_1} & \frac{\partial f_l}{\partial z_2} & \cdots & \frac{\partial f_l}{\partial z_k} \end{bmatrix} = \left[\frac{\partial f_i}{\partial z_j}\right]_{k\times l}. \tag{10}$$

where l is the number of the pixels, k is the number of DM actuators, and $i = 1, 2\cdots, l$; $j = 1, 2\cdots, k$, z_j represents the voltage of jth DM acutuator.

We approximate the partial derivative in the Jacobian as

$$\frac{\partial f_i}{\partial z_j} \approx \frac{f_i(z_1, z_2, \cdots, z_j + \Delta z, \cdots, z_k) - f_i(z_1, z_2, \cdots, z_j, \cdots, z_k)}{\Delta z}. \tag{11}$$

where Δz is a small increment of the voltage. Notice that $\frac{\partial f_i}{\partial z_j}$ represents the element J_{ij} in Jacobian $J = \frac{\partial(f_1, f_2, \cdots, f_l)}{\partial(z_1, z_2, \cdots, z_k)}$.

In general, the convergence speed of Newton iteration is relatively fast, it can converge after two or three iterations. We can use Eq. (9) to update the voltage of the actuators until $RMS(f^{n+1} - f^n) < \varepsilon$, where ε is the predefined converging threshold of iteration, i.e., $0.001\mu m$, f represents the tested phase distribution calculated from the interferograms, and n represents the number of iterations.

After the three steps of optimizations, the approximate no-fringe interferogram can be obtained, and the phase distribution of the freeform surface under test can be calculated.

4. Simulation of driving algorithm

To validate the performance of the driving algorithm, we perform two groups of simulations. One phase distribution is generated by the response matrix of DM since we want to verify the effectiveness of the driving algorithm, and the other phase distribution is generated by the Zernike polynomials. Note that, we can't simulate the first step since the relatively dark region without fringe can't be simulated, we can only simulate the second and third optimization steps.

Figs. 2 and 3 are the simulated results between the second and final steps when the tested phase distribution is generated by the response matrix of DM. Fig. 2(a) is the original interferogram, after the SPGD optimization ($\delta U = 0.01$, $\gamma = 200$), the interferogram becomes Fig. 2(b), and the convergence curve is shown in Fig. 3(a), we can see that the fringe density in the interferogram decreases after the SPGD optimization, and SPGD algorithm can converge through a relatively large number of iterations. After this step, we can calculate the RMS value of the phase distribution from Fig. 2(b) directly and use it as the system performance metric in the final step, in order to demonstrate the performance of the Newton iteration algorithm, we separately use the Newton iteration and SPGD algorithms to optimize Fig. 2(b) in the final step, the optimized interferograms after using the Newton iteration and SPGD algorithms are shown in Fig. 2(c) and (d) respectively, and the convergence curves are plotted in Figs. 3(b) and (c). It is clear that the Newton iteration algorithm can converge to the minimum value quickly (Fig. 3(b)), and the interferogram can achieve ideal no-fringe (Fig. 2(c)), but the RMS value of phase distribution can be only converged to 0.4959 μm by further using SPGD algorithm (Fig. 3(c)) and the fringe density of the optimized interferogram (Fig. 2 (d)) is still relatively high. This simulation demonstrates that, in the final step, the Newton iteration algorithm has the better performance than the SPGD algorithm.

As a second example, we simulate the phase distribution with the Zernike polynomials. The original interferogram is shown in Fig. 4 (a), the fringe density is relatively high. With SPGD optimization ($\delta U = 0.01$, $\gamma = 200$), we can see that the fringe becomes more sparse as shown in Fig. 4(b), and the convergence curve is relatively flat after 100 iterations (Fig. 5(a)). Similarly we also use Newton iteration and SPGD algorithms separately to optimize Fig. 4(b). After two iterations (Fig. 5(b)), the RMS value of the phase distribution using Newton iteration algorithm can't be reduced to zero, but to a minimum value ($RMS = 0.0186\mu m$), the interferogram is shown in Fig. 4(c). However, SPGD algorithm cannot further reduce RMS value to approximately zero (Fig. 5(c)) and the fringe density in the interferogram almost remains the same (Fig. 4(d)).

In the above two simulations, we use the same gain coefficient γ and random turbulence voltage δU in the second step, and the results both converge since the proportion of the number of the different symbols to the number of the effective points in the interferogram is used as the system performance metric, the value of J changes slightly due to the different interferograms, however, if we use the number of the different symbols between $I'(i, j)$ and $I'(i, j+1)$ or $I'(i+1, j)$ in the interferogram as the system performance metric, the value of J will change enormously, the gain coefficient needs to be changed with the different situations, otherwise, the optimization may be too early convergence, slow convergence or no convergence. In the following, we will compare the results of these two different system performance metrics.

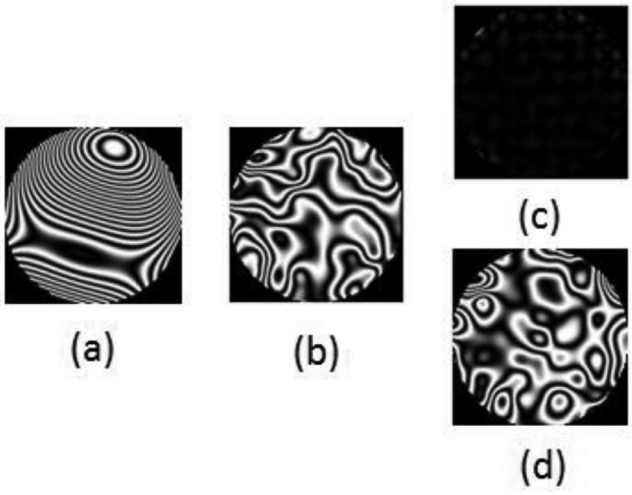

Fig. 4. Simulated interferograms between the second and final steps when the tested phase distribution is generated by the Zernike polynomials. (a) The original interferogram, (b) the interferogram after using SPGD algorithm (second step), (c) and (d) the final interferogram after further using Newton iteration and SPGD algorithms (final step).

We simulate 5 groups of phase distributions with different RMS values, and two different system performance metrics are used to optimize the interferogram in the second step, Fig. 6 (a) describes the convergence curves with different phase distributions when the proportion is used as the system performance metric, we can see that all the simulations can converge very well even use the same gain coefficients, different phase distributions don't affect the convergence, Fig. 6 (b) shows the convergence curves with different phase distributions when the number of the different symbols is used as the system performance metric, not all the optimizations converge, only the optimizations with $RMS = 2.8507\mu m$ and $RMS = 3.0289\mu m$ can converge very well, for $RMS = 2.1173\mu m$ and $RMS = 1.8846\mu m$, the results are too early convergence, and for $RMS = 1.5573\mu m$, the result is no convergence, hence, if we use the number as the system performance metric, we need to change the gain coefficient according to the different situations to ensure the good convergence. Through the comparison, the proportion is more suitable to be the system performance metric than the number in the second step.

5. Experiment

To demonstrate the proposed driving algorithm of DM, we measured an unknown freeform surface. Fig. 7(a) is the interferogram when DM is flat, there is no fringe in the upper right region of the interferogram. In the first step, the relatively dark domain without fringe as identified, and the grayscale values of the interferogram were normalized to easily calculate the sum of grayscale values, then the SPGD algorithm was applied ($\delta U = 0.01$, $\gamma = 200$), the no-fringe region was recovered as shown in Fig. 7 (b). From the convergence curve in Fig. 8(a), we can see that the sum of the grayscale values increased with the recovery of the fringe, and the SPGD algorithm converged after 50 iterations. After the first step, the fringe density was still relatively high and should be relaxed, then the SPGD algorithm was also used in the second step, after 100 iterations, the fringe in the interferogram became sparse, as shown in Fig. 7(c), and the SPGD algorithm converged as shown in Fig. 8(b). Through the simulation, we knew that the Newton iteration algorithm is better than the SPGD algorithm in the final step, so we used the Newton iteration algorithm to optimize the interferogram in Fig. 7(c), the approximate no-fringe interferogram was obtained, as shown in Fig. 7(d). From the convergence curve in Fig. 8(c), we can see that the Newton iteration algorithm can achieve fast convergence, and it can converge to a minimum value ($RMS = 0.1815\lambda$, $\lambda = 0.6328\mu m$), the interferogram

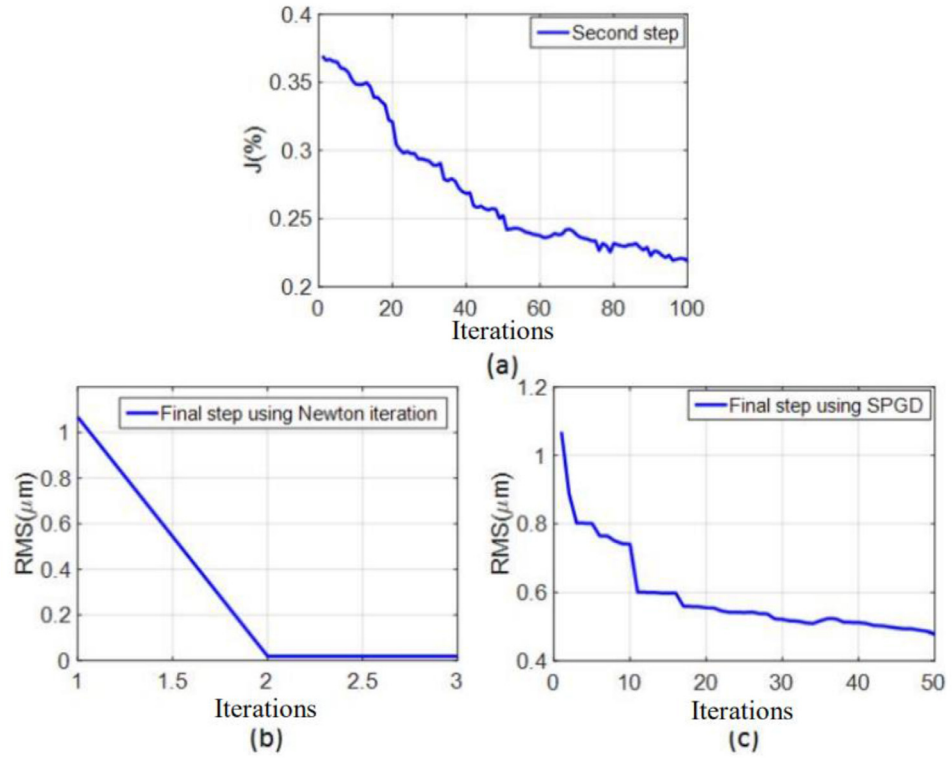

Fig. 5. Simulated convergence curves between the second and final steps when the tested phase distribution is generated by the Zernike polynomials, (a) The convergence curve using SPGD algorithm (second step), (b) and (c) the convergence curves using Newton iteration and SPGD algorithms (final step).

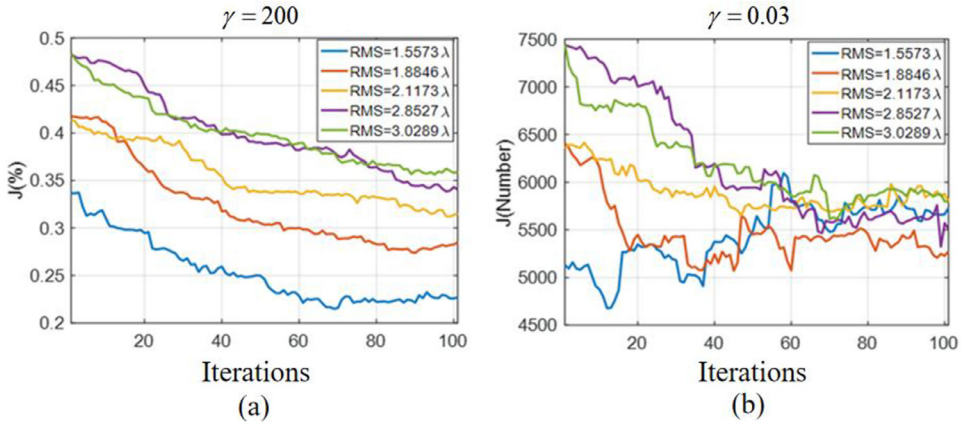

Fig. 6. Simulated convergence curves with different phase distributions and system performance metrics. (a) The convergence curves with different phase distributions using the proportion as the system performance metric, (b) the convergence curves with different phase distributions using the number of the different symbols as the system performance metric.

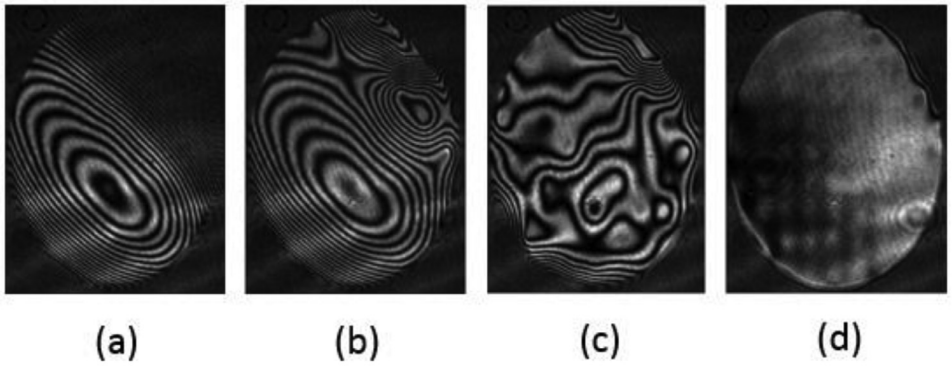

Fig. 7. Experimental interferograms between the first and final steps. (a) The original interferogram, (b) the interferogram after recovering dark domain without fringe by SPGD algorithm (first step), (c) the interferogram after using SPGD algorithm (second step), (d) the interferogram after using Newton iteration algorithm (final step).

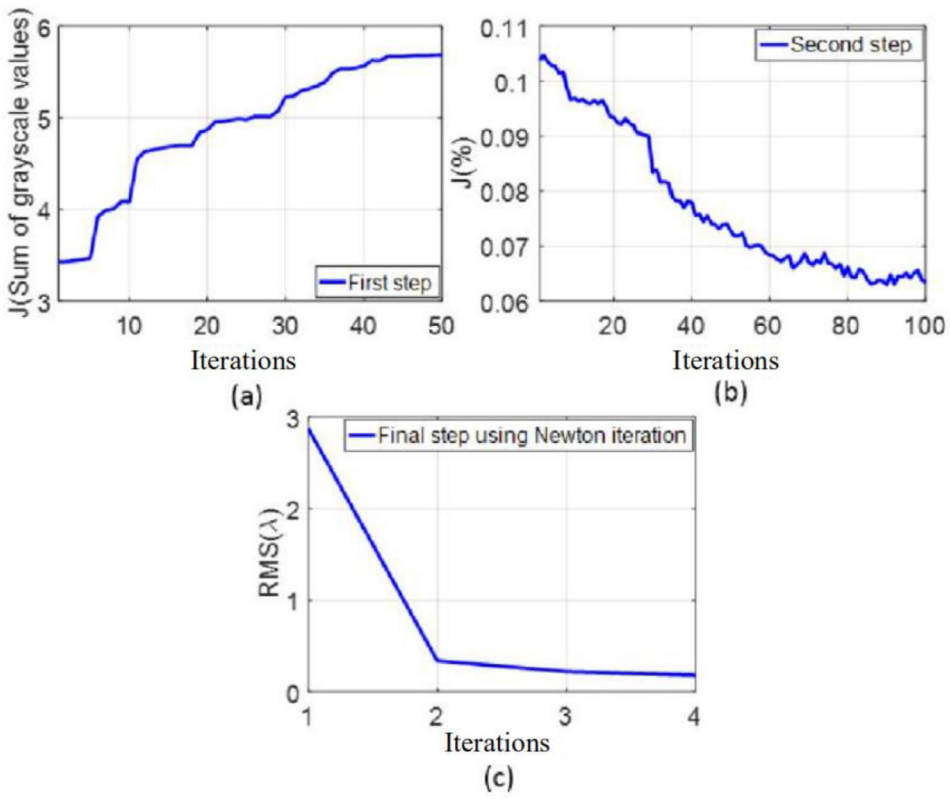

Fig. 8. Experimental convergence curves between the first and final steps. (a) The convergence curve using SPGD algorithm (first step), (b) the convergence curve using SPGD algorithm (second step); (c) the convergence curve using Newton iteration algorithm (final step).

is not perfect no-fringe since the original phase distribution is not generated by controlling the actuators of the DM as the second simulation, however, it doesn't affect the accurate calculation of the phase distribution.

6. Conclusion

In this paper, we introduce the principle of the adaptive interferometer firstly, then a SPGD and Newton iteration mixed algorithm has been developed to drive the DM in the adaptive interferometer. The SPGD algorithm first recovers the relatively dark region of the interferogram and then reduces the fringe density, the Newton iteration algorithm is utilized in the final step to obtain the nearly no-fringe interferogram, these three steps use the different system performance metrics. We have demonstrated the proposed DM driving algorithm with the simulated data and experimental data. This algorithm has the potential application in freeform surface metrology.

Funding

This work was supported by the National Natural Science Foundation of China (NSFC) (61905039); Jilin Scientific and Technological Development Program (20190701018GH); Education Department of Jilin Province (JJKH20190691KJ) and State Key Laboratory of Applied Optics.

Declaration of Competing Interest

The authors declare that they have no known competing financial interests or personal relationships that could have appeared to influence the work reported in this paper.

CRediT authorship contribution statement

Yu Zhang: Conceptualization, Methodology, Formal analysis, Writing - review & editing, Funding acquisition. **Xiaobo Tian:** Investigation, Data curation, Software. **Rongguang Liang:** Writing - review & editing.

References

[1] Ma D, Feng Z, Liang R. Freeform illumination lens design using composite ray mapping. Appl Opt 2015;54:498–503. https://doi:10.1364/ao.54.000498.
[2] Blalock T, Medicus K, Nelson JD. Fabrication of freeform optics. Proc SPIE 2015;9575:95750H. https://doi.org/10.1117/12.2188523.
[3] Garbusi E, Pruss C, Osten W. Interferometer for precise and flexible asphere testing. Opt Lett 2008;33(24):2973–5. https://doi:10.1364/ol.33.002973.
[4] Schindler J, Baer G, Pruss C, Osten W. The tilted-wave-interferometer: freeform surface reconstruction in a non-null setup. Proc SPIE 2014;9297:92971R. https://doi.org/10.1117/12.2073053.
[5] Chen S, Li S, Dai Y, Zheng Z. Testing of large optical surfaces with subaperture stitching. Appl Opt 2007;46(17):3504–9. https://doi:10.1364/ao.54.000498.
[6] Stuerwald S. Error compensation in computer generated hologram-based form testing of aspheres. Appl Opt 2014;53(35):8249–55. https://doi:10.1364/ao.53.008249.
[7] Park J, Kwon K, Cho N. Development of a coordinate measuring machine (CMM) touch probe using a multi-axis force sensor. Meas Sci Technol 2006;17:2380–6. doi:10.1088/0957-0233/17/9/002.
[8] Aceves-Campos H. Profile identification of aspheric lenses. Appl Opt 1998;37(34):8149–50. https://doi:10.1364/ao.37.008149.
[9] Nadim E, Hichem N, Nabil A, Mohamed D, Olivier G. Comparison of tactile and chromatic confocal measurements of aspherical lenses for form metrology. Int J Precis Eng Man 2014;15:821–9. https://doi:10.1007/s12541-014-0405-y.
[10] Fuerschbach K, Thompson KP, Rolland JP. Interferometric measurement of a concave, φ-polynomial, Zernike mirror. Opt Lett 2014;39(1):18–21. https://doi:10.1364/ol.39.000018.
[11] Huang L, Choi H, Zhao W, Graves LR, Kim DW. Adaptive interferometric null testing for unknown freeform optics metrology. Opt Lett 2016;41(23):5539–42. https://doi:10.1364/ol.41.005539.
[12] He Y, Huang L, Hou X, Fan W, Liang R. Modeling near-null testing method of a freeform surface with a deformable mirror compensator. Appl Opt 2017;56(33):9132–8. https://doi:10.1364/ao.56.009132.
[13] Vorontsov MA. Stochastic parallel-gradient-descent technique for high-resolution wave-front phase-distortion correction. J Opt Soc Am A 1998;15:2745–58. https://doi:10.1364/josaa.15.002745.

[14] Qi Z, Xiao L, Fu S, Li T, Jiang G, Long X. Two-step camera calibration method based on the SPGD algorithm. Appl Opt 2012;51(26):6421–8. https://doi:10.1364/ao.51.006421.
[15] Yazdani R, Hajimahmoodzadeh M, Fallah HR. Adaptive phase aberration correction based on imperialist competitive algorithm. Appl Opt 2014;53(1):132–40. https://doi:10.1364/ao.53.000132.
[16] Wu K, Sun Y, Huai Y, Jia S, Chen X, Jin Y. Multi-perturbation stochastic parallel gradient descent method for wavefront correction. Opt Express 2015;23(3):2933–44. https://doi:10.1364/oe.23.002933.
[17] Ma H, Xie Z, Long X, Qi B, Ren G, Shi J, Cui Z, Jiang Y, Xu X. Synthetic aperture imaging by using spatial modulation diversity technology with stochastic parallel gradient descent algorithm. Opt Express 2015;23(11):14836–49. https://doi:10.1364/oe.23.014836.
[18] Tian X, Tu X, Zhang J, Spires O, Brock N, Pau S, Liang R. Snapshot multi-wavelength interference microscope. Opt Express 2018;26(14):18279–91. https://doi:10.1364/oe.26.018279.
[19] Huang L, Xue J, Gao B, McPherson C, Beverage J, Idir M. Modal phase measuring deflectometry. Opt Express 2016;24(21):24649–64. https://doi:10.1364/oe.24.024649.
[20] Huang L, Zhou C, Zhao W, Choi H, Graves L, Kim D. Close-loop performance of a high precision deflectometry controlled deformable mirror (DCDM) unit for wavefront correction in adaptive optics system. Opt Commun 2017;393:83–8. https://doi:10.1016/j.optcom.2017.02.003.
[21] Ben-Isreal A. A Newton-Raphson method for the solution of systems of equations. J Math Anal Appl 1966;15(2):243–52. https://doi:10.1016/0022-247x(66)90115-6.